ELSEVIER

Catalysis Today 53 (1999) 35–50

CATALYSIS TODAY

www.elsevier.com/locate/cattod

Catalytic hydrogenation of aqueous nitrate solutions in fixed-bed reactors

Albin Pintar *, Jurka Batista

Laboratory for Catalysis and Chemical Reaction Engineering, National Institute of Chemistry, Hajdrihova 19, P.O. Box 3430, SI-1001 Ljubljana, Slovenia

Abstract

Liquid-phase hydrogenation using a solid Pd–Cu bimetallic catalyst offers a promising technique for the removal of nitrates from contaminated drinking water. In this study, catalytic nitrate reduction was investigated in isothermal fixed-bed reactors at $T = 298$ K and atmospheric pressure. Experiments carried out in a bubble-column fixed-bed reactor in the presence of distilled water as a reaction medium, demonstrate that nitrates can be efficiently removed from the liquid-phase, and that the maximum contaminant level for ammonium ions in drinking water is not exceeded. The measured nitrate conversions are considerably influenced by the variation of volumetric flow rate of either the gas- or liquid-phase. The order of magnitude analysis of apparent rate constant and mass transfer coefficients confirms that the observed reaction rate is governed by the mass transfer of hydrogen from the gas- into the bulk liquid-phase. Due to shorter mean residence times, lower nitrate conversions are measured in a trickle-bed reactor. At the given reaction conditions, catalyst particles were directly exposed to the gas-phase in this reactor system, which drastically enhanced ammonia production. When drinking water is used as a reaction medium instead of distilled water, the nitrate disappearance rate as well as reaction selectivity decrease appreciably, which is attributed to the presence of dissolved ionic species. Additionally, traces of nitrites were detected in the reactor effluent.

Keywords: Aqueous solution, Bubble-column fixed-bed reactor, Catalytic liquid-phase hydrogenation, Drinking water purification, Heterogeneous catalysis, Nitrate removal, Pd–Cu bimetallics, Reaction kinetics, Reaction selectivity, Trickle-bed reactor

1. Introduction

Nitrate concentrations in surface water and especially in ground water have increased in many locations in the world. Man-made or man-caused sources of nitrogen introduction into the subsurface environment include agricultural fertilizers, septic tank systems, and animal waste disposal. Since nitrates cause methemoglobinemia in infants, increased nitrate concentrations in ground water have led to the shutdown of wells and rendered aquifers unusable as water sources. Communities with closed nitrate-contaminated wells now need them to meet the increased water demand. Surface waters also have experienced seasonal nitrate violations. As a result, there is renewed interest in the removal of nitrates from raw water.

Removal of nitrates from drinking water is an important and developing area of research. Although technology in this area is developing, there is still a need to further optimize the current treatment techniques and develop the emerging processes for

* Corresponding author. Tel.: +386-61-17-60-282; fax: +386-61-12-59-244
E-mail address: albin.pintar@ki.si (A. Pintar)

0920-5861/99/$ – see front matter
PII: S0920-5861(99)00101-7

nitrate remediation. In a recent paper of Kapoor and Viraraghavan [1], the present state-of-the-art of treatment methods for the removal of excessive quantities of nitrate ions from drinking water is discussed, and various treatment options are compared in terms of their effectiveness, ease of operation, and cost. The most promising techniques for nitrate removal, without any occurrence of wastewater, are biological digestion and catalytic denitrification by using noble metal catalysts [2–4]. The main reasons for the slow transfer of biological denitrification to drinking water purification are concerns over possible bacterial contamination of treated water, the presence of residual organics in treated water, and the possible increase in chlorine demand of purified water. Furthermore, the presence of old sludge could lead to the formation of nitrites. The reduction of aqueous nitrate solutions by using hydrogen over a solid catalyst offers an alternative and economically advantageous process to biological treatment as a means of purifying drinking water streams. The reaction obeys a consecutive reaction scheme in which the nitrite appears as an intermediate, while nitrogen and ammonia are the final products. To maintain electroneutrality of the aqueous phase, consumed nitrates are replaced by hydroxide ions. Supported Pd–Cu, Pd–Sn and Pd–In bimetallic catalysts promote nitrate reduction in spite of inadequate selectivity towards nitrogen production [4,5]. Since the described technique is in a stage of development, further kinetic and mechanistic studies with different systems in aqueous solutions are needed.

A detailed kinetic model of the catalytic nitrate reduction was recently derived by Pintar et al. [6]. The results of investigations carried out in an isothermal semi-batch slurry reactor show that the rate of nitrate disappearance is well described by a rate equation of Langmuir–Hinshelwood type, which accounts for both noncompetitive and equilibrium nitrate and dissociative hydrogen adsorption steps, as well as the irreversible bimolecular surface process that controls the overall reaction rate. The observed kinetics in the slurry reactor are not influenced either by the presence of nitrites as intermediates, or by ammonium ions as a side product in the reduction route towards nitrogen formation. It was discovered in a series of runs using various nitrate salts as sources of nitrate ions that the apparent surface reaction rate constant increases in the order $K^+ < Na^+ < Ca^{2+} < Mg^{2+} < Al^{3+}$ and changes proportionally with the ionization potential of the cations present in the aqueous solution [7]. The permanent hardness of drinking water exhibits no inhibitive impact either on the extent of nitrate removal or on reaction selectivity. On the other hand, the nitrate disappearance rate as well as the nitrogen production yield decrease appreciably in the presence of hydrogencarbonates.

To the best of our knowledge, the process of catalytic liquid-phase nitrate reduction has so far been studied in detail in batch reactors; no investigations have been published on the reduction of nitrates in conventional three-phase reactors. Sell et al. [8] carried out the catalytic nitrate reduction in pilot fixed-bed and expanded-bed reactors. The units operated at a temperature of ground water and total pressures up to 6 bar over an alumina supported Pd–Cu bimetallic catalyst containing 2.0 wt.% of Pd and 0.5 wt.% of Cu metallic phases. Hydrogen was used as a reducing agent and predissolved in the liquid-phase prior to entering into the denitrification reactor; due to the elevated operating pressure, single-phase flow was established in the catalytic bed. With an expanded-bed reactor, rates of nitrate reduction of up to 2.5 g/kg catalyst per hour were achieved. On the other hand, the nitrate disappearance rate measured in the 'liquid-full' fixed-bed reactor was lower by about five times, which is attributed to mass-transfer limitations. It is furthermore reported by Sell et al. [8] that neither any accumulation of intermediate nitrites nor the formation of ammonium ions has been observed. The objective of the present work is to examine the catalytic liquid-phase reduction of aqueous nitrate solutions in continuous-flow three-phase reactors with respect to the extent of total remediation and reaction products formed during the reaction course in the presence of various Pd-Cu/γ-Al_2O_3 bimetallics. Nitrate remediation was studied in isothermal bubble-column fixed-bed and trickle-bed reactors operating on integral level in a wide range of operating conditions. A few reduction runs were carried out by using tap water instead of distilled water in order to evaluate the potential of the catalytic denitrification technique for drinking water purification. Finally, the chemical stability of the catalysts under the reaction conditions was studied.

2. Experimental

2.1. Catalyst synthesis and characterization

Three Pd-Cu/γ-Al_2O_3 precursors with various Pd and Cu contents were prepared by incipient-wetness successive impregnation of γ-Al_2O_3 spheres (Nikki Universal, NST-5 type; BET surface area: 172 m^2/g; total pore volume: 1.02 cm^3/g, average pore diameter: 16.1 nm, particle density: 0.80 g/cm^3, solid density: 4.25 g/cm^3 (all determined by the Mercury Porosimetry method on a Micromeritics Pore Sizer 9310 instrument); iep: 8.3; average sphere diameter: 1.70 mm) using aqueous $Cu(NO_3)_2 \cdot 3H_2O$ (Merck, p.a., 99.5 wt.%) and $Pd(NO_3)_2 \cdot 2H_2O$ (Fluka, p.a., 40 wt.% Pd) solutions. For catalyst preparation, the support was heated to 523 K prior to impregnation in order to remove adsorbed moisture. The dried γ-Al_2O_3 spheres were impregnated first with the copper salt, which was then slowly oven-dried overnight at 423 K and calcined at 773 K for 1 h in dry air. The obtained solid was further impregnated with an aqueous solution of palladium nitrate. After slowly drying at 423 K, the obtained solid was calcined at 773 K for 3 h in dry air and finally reduced in hydrogen atmosphere for 1 h at the same temperature. The concentrations of metallic Pd and Cu phases were in the range 0.1–1.0 wt.% and 0.03–0.3 wt.%, respectively. The concentrations of the metallic palladium and copper phases (ICP-AES analysis) and the surface area (BET method) of the catalysts are given in Table 1.

Scanning electron microscopy and energy-dispersive X-ray spectroscopy (EDX) were carried out in a Jeol 5800 scanning electron microscope equipped with the Oxford Instruments Link Isis Model L300 EDX system. For secondary electron (SE) and back-scattered electron imaging of catalyst particles, the powders were coated with a thin layer of gold. For microanalysis, polished flat surfaces of the catalysts were prepared by conventional metallographic techniques. The powders were embedded in epoxy resins, ground on SiC papers and afterwards polished with 3 and 0.5 μm diamond pastes. The specimens were coated with a thin graphite layer in order to ensure electrical conductivity of the surface. The working conditions for EDX analysis were set to 20 kV voltage and ~0.5 nA beam current. The maximum depth analyzed under these conditions is about 1 μm. EDX spectra were acquired in two ways, either by positioning the beam (diameter ~0.2 μm) in spot mode to the area of interest or by performing linescans across the polished particles of the catalyst. In the first case the EDX spectra were acquired for 100 s. The analogue linescans were acquired in subsequent frames until a sufficient signal to noise ratio was obtained.

Table 1
Properties of the support and hydrogenation catalysts

Catalyst	c_{Pd}, wt.%	c_{Cu}, wt.%	S_{BET}, m^2/g
γ-Al_2O_3	–	–	172
CAT-1	1.0	0.3	162
CAT-2	0.5	0.15	161
CAT-3	0.1	0.03	162

2.2. Apparatus and experimental procedure

In this study, catalytic nitrate reduction was carried out in isothermal bubble-column fixed-bed and trickle-bed reactors. The upflow/downflow reactor was made of a 50 cm section of 20 mm I.D. glass tubing and equipped with a heating/cooling jacket. The liquid feed solution with a known concentration of nitrate ions was prepared from distilled water and reagent grade KNO_3 and maintained saturated with hydrogen by bubbling a H_2–CO_2 mixture through the feed reservoir. Gas-flow rates were controlled by electronic mass flow controllers (MKS). A thermostat (Haake, model DC3/K20) and recirculating pump were installed to maintain constant temperature in the feed reservoir. The liquid with predissolved hydrogen was fed either upflow or downflow into the reactor by means of a positive displacement pump (LDC, model 3200). The gas stream was a H_2–CO_2 mixture, which was fed to the bottom (bubble-column fixed-bed) or top (trickle-bed) of the reactor. CO_2 was employed as a hydrogen diluting agent in order to eliminate the influence of the produced hydroxide ions on the reaction course. The gas- and liquid-phases passed through a distributor and the bed of catalyst spheres in a co-current mode. The flow rate of the gas mixture introduced into the reactor was controlled by electronic mass flow controllers (MKS). In this work, the reactor was filled with 25 g of the catalyst. The fixed-bed was supported by a stainless-steel screen placed near the bottom of

Table 2
Experimental conditions of the catalytic liquid-phase nitrate hydrogenation in fixed-bed reactors

Mass of catalyst in bed, g	25.0
Catalyst bed length, cm	16.5
Bed density, g/cm^3	0.46
Bed porosity, dimensionless	0.43
Catalyst particle diameter, mm	1.70
Particle density, g/cm^3	0.80
Reaction temperature, K	298
Total operating pressure, bar	1.0
Hydrogen partial pressure, bar	0–0.5
Gas flow rate, ml/min	20–160
Liquid flow rate, ml/min	4.0–10.8
Nitrate feed concentration, mg/l	60.0–100.0

Table 3
Composition of tap water used as a reaction medium in the process of catalytic liquid-phase nitrate hydrogenation

Component	Concentration (mg/l)
Potassium (K^+)	1.5
Sodium (Na^+)	5.7
Ammonium NH_4^+	0.05
Calcium (Ca^{2+})	105.0
Magnesium (Mg^{2+})	22.8
Chloride (Cl^-)	11.5
Hydrogencarbonate (HCO_3^-)	316.6
Nitrate (NO_3^-)	47.7
Nitrite (NO_2^-)	<0.005
Sulfate SO_4^{2-}	36.5
Total organic carbon (TOC)	1.1

the reactor tube. Glass spheres (d_p: 1 mm) were placed below and above the catalyst bed in order to improve the liquid distribution, and to reduce channelling and dead volume. The reactor effluent was separated into the gas- and liquid-phase in an upper/bottom part of the reactor tube. To monitor the progress of the reaction under consideration, representative liquid-phase samples were collected at the top or bottom of the reactor and analyzed for residual nitrate concentration, as well as nitrite and ammonium ion contents. The properties of the catalyst bed and the reactor operating conditions are listed in Table 2.

Temperatures were measured with iron-constantan thermocouples (J-type) placed at the bottom and top of the catalyst bed. No temperature rise, due to the heat of reaction, was observed in any of the runs, since the reactor operated with low nitrate feed concentrations (up to 100 mg/l). The temperature of the reactor was successfully controlled within ±0.10 K of the set value (Haake, model DC3/K20), which confirms that the reactor was operated isothermally. No pressure control was required since the total operating pressure was equal to atmospheric pressure.

A few reduction runs were conducted in which tap water was used as a reaction medium instead of distilled water in order to evaluate the potential of the catalytic denitrification technique for drinking water purification. The composition of tap water is given in Table 3.

2.3. Analysis

The concentrations of nitrate ions in the aqueous-phase samples were determined by means of a UV/VIS spectrophotometer (Perkin-Elmer, model Lambda 40P) combined with the X-Y autosampler and flow-injection analyzer (Perkin-Elmer, model FIAS 300). A flow cell with a volume of 18 μl and optical pathlength of 10 mm was installed in the sample compartment of the UV/VIS spectrophotometer, thus enabling instantaneous response. The nitrate ions analysis was carried out in the UV-range at $\lambda = 220$ nm. Distilled water was used as a mobile phase, and the flow rate of the latter was set to 240 ml/h in order to ensure linear system response in the concentration range 0–250 mg/l of nitrates. Reagents containing diluted perchloric (2.5 wt.%) and amidosulphuric (1.0 wt.%) acids were employed as a means to eliminate any effect of the present nitrite ions on the measured absorbances [9]. The flow of the mobile phase and reagents through the tubing and loops was arranged in such a way that a sample was injected accordingly to the branched F(low) I(njection) A(nalysis) technique. For the described analytical method, the relative analysis error was found to be below 0.5%. To evaluate concentrations of nitrite and ammonium ions, the 'naphthylamine' and 'gas-diffusion/acid–base indicator' analytical procedures were applied using the same apparatus [10]. In order to check for any evolution of hydroxylamine during the catalytic nitrate reduction, aqueous-phase samples were further analyzed following the procedure proposed by Johnson [11]. The pH values of the samples were determined by employing a digital pH meter (Metrohm, model 751 GPD Titrino) equipped with a 'Long-Life' combination electrode and Pt-1000 temperature sensor.

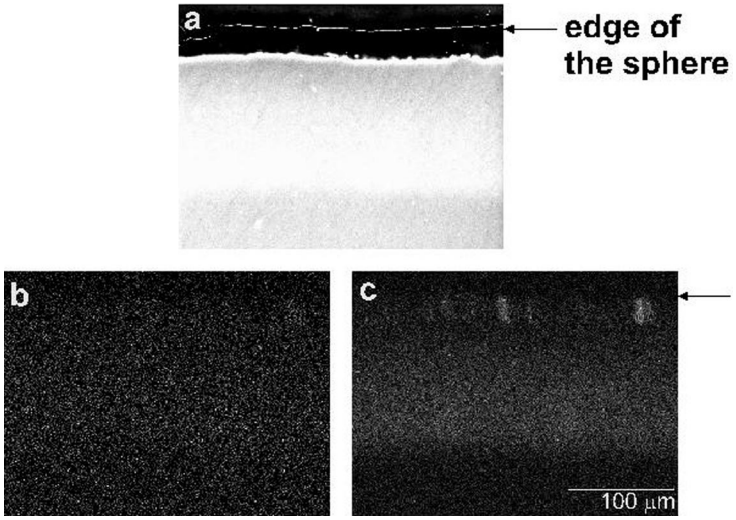

Fig. 1. Electron probe microanalysis of the Pd (1.0 wt.%)–Cu(0.3 wt.%)/γ-Al_2O_3 CAT-1 sample: SEM image of the area analyzed (a); X-ray maps of Cu (b) and Pd (c), respectively.

3. Results and discussion

Energy Dispersive System mapping of Cu and Pd, determined on sections of several CAT-1 spheres (Fig. 1) revealed uniform distribution of copper in the analyzed layers (200 μm). It is evident that in comparison to Cu, palladium is dispersed in the narrower outer layers. In order to get more information about the location of active phases within the support, EDX linescan analysis was applied. The results are illustrated in Fig. 2. It can be seen that Pd is found in depths up to 120 μm. Due to a lower concentration, the EDX spectrum of Cu is less revealing. By means of deconvolution, the depth of copper penetration was found to be 200 μm, which is consistent with the result shown in Fig. 1. Based on the above findings, it can be concluded that the reaction zone for nitrate reduction, composed of both Pd and Cu atoms [12], is 120 μm thick. A comparison of EDX linescan spectra of samples in reduced and oxidic (not shown here) form demonstrates that Pd and Cu atoms diffuse towards the catalyst surface during the reduction at 773 K; however, due to a lower sublimation heat (or lower surface energy) this effect is more pronounced for copper.

3.1. Bubble-column fixed-bed reactor (BCFR)

Fig. 3 shows the influence of volumetric gas flow rate on the outlet nitrate concentration and the content of produced ammonium ions in the BCFR reactor over the CAT-1 sample in the presence of distilled water as

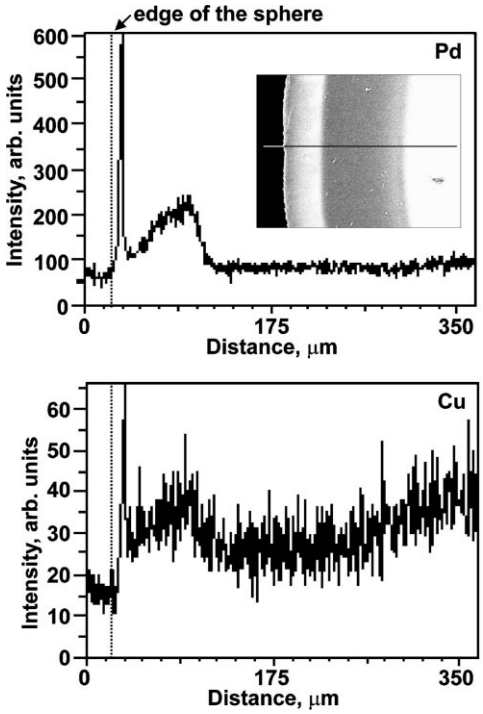

Fig. 2. Results of EDX line analysis of the cross section of CAT-1 sample. The SEM micrograph of the cross section of the catalyst sphere is inset in the upper spectrum.

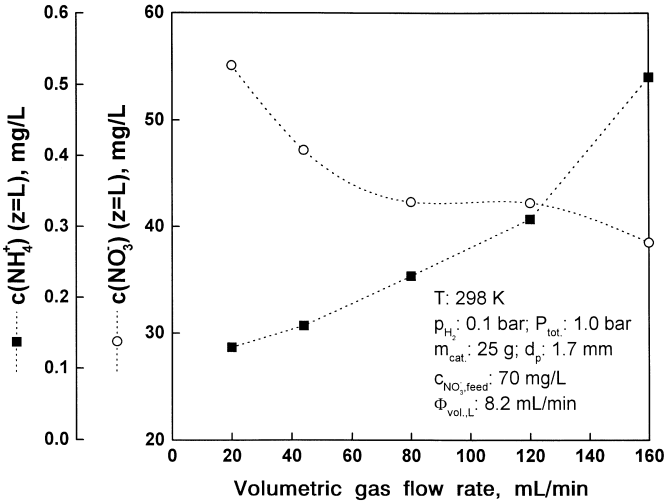

Fig. 3. Nitrate and ammonium ions concentration as a function of volumetric gas flow rate obtained in the bubble-column fixed-bed reactor over the CAT-1 sample.

a reaction medium. It can be seen that at the employed reaction conditions, the measured nitrate concentrations for any gas flow rate, except $\Phi_{vol.,G} = 20$ ml/min, is lower than the maximum admissible concentration for drinking water (i.e., 50 mg/l). Due to the low hydrogen partial pressure (0.1 bar) used in these runs, the amounts of ammonium ions formed in the process of catalytic nitrate hydrogenation carried out in the BCFR reactor were found to be below the maximum contaminant concentration (i.e., 0.5 mg/l). At the given operating conditions, no nitrite was detected in the reactor effluent, and up to 3.5 mol% of consumed nitrates were found in the form of ammonium ions. Furthermore, the $c_{NO_3^-}$ vs. $\Phi_{vol.,G}$ dependence in Fig. 3 forms a S-shaped curve, which is due to: (i) the increase of gas-liquid interfacial area, a_G, with an increase of volumetric gas flow rate (Fig. 4a); (ii) the simultaneous decrease of liquid hold-up in the reactor, while increasing $\Phi_{vol.,G}$ (Fig. 4b). The dependencies plotted in Fig. 4 were calculated by means of correlations proposed by Marquez et al. [13] and Larachi et al. [14]. One should note that these correlations were obtained in a laboratory-scale BCFR reactor with packings, the dimensions of which are similar to those of our experimental set-up and catalyst particles. Fig. 4a shows values of the gas–liquid interfacial area (a_G) which are an order of magnitude lower than the area available for liquid–solid mass transfer (a_S). In case the reactor operates in the mass-transfer regime, one can suppose that the overall nitrate disappearance rate is determined by the mass transfer of the gaseous reactant into the bulk liquid-phase. Based on the dependencies illustrated in Fig. 4b, the mean residence time of the liquid-phase for any of the reduction runs carried out in the BCFR reactor was estimated to be in the range 1.3–3.3 min. The hydrodynamic pattern found in the BCFR reactor during catalytic nitrate reduction was rather complex. When the flow of both the gas and the liquid is regular (i.e., no pulsation, churn, or any flow maldistribution), the following two limiting flow patterns can be considered: bubble flow and continuous gas streams flowing through wet bed voids. In the bed under our conditions, significant maldistribution of the two-phase upflow was observed. There was neither any 'pure' bubble flow nor full channelling; part of the voids was completely filled with liquid, and in others channelling occurred. This finding is in agreement with the recent results of Molga and Westerterp [15,16], who report that for small particles (d_p below 10 mm) flow maldistributions are enhanced, resulting in pure gas flow in part of the voids, and in simultaneous gas-liquid flow in the others.

The effect of the volumetric liquid flow rate on the reaction course is shown in Fig. 5a, where nitrate conversion is plotted as a function of the $m_{cat.}/\Phi_{vol.,L}c_{NO_3^-,feed}$ ratio. The measured nitrate

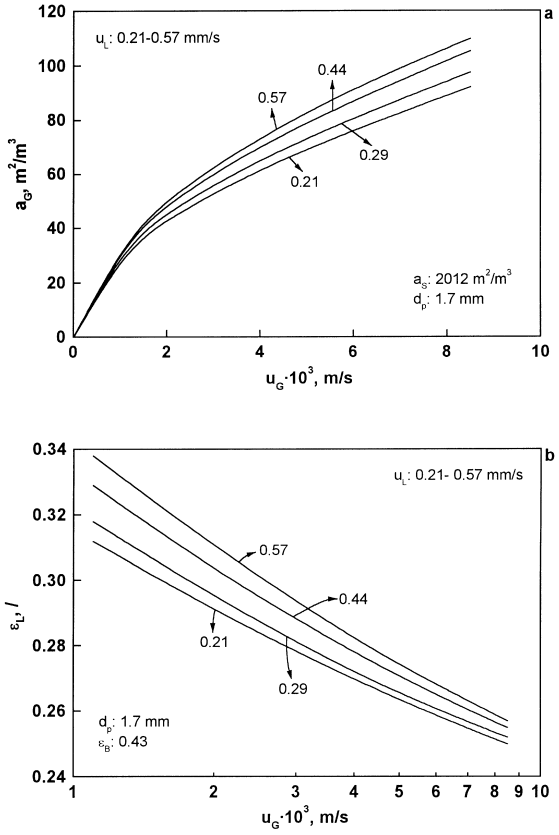

Fig. 4. Interfacial gas–liquid area (a) and liquid hold-up (b) as a function of the superficial gas velocity for different superficial liquid velocities.

conversions decrease with an increase of liquid flow rate. Although the values of mass-transfer coefficients and liquid hold-up are higher at increased liquid flow rates, their contribution to the extent of reaction is overcome by a drop of the mean residence time of the liquid-phase in the fixed bed. It is further seen from Fig. 5b that for the selected range of volumetric liquid flow rates, except $\Phi_{vol.,L} = 4.0$ ml/min, the concentrations of ammonium ions found in the reactor effluent are below the maximum contaminant level. At these reaction conditions, it was found that up to 3.5 mol% of nitrates is again reduced to ammonium ions. It can be thus concluded that the relative amount of nitrates converted to ammonia is mainly dependent on hydrogen partial pressure.

Fig. 3a demonstrates that the measured nitrate conversions in the reactor effluent are considerably influenced by the variation of volumetric gas flow rate. This suggests that the reaction under consideration is affected by the mass-transfer of hydrogen to Pd–Cu active sites on the catalyst surface. To prove this hypothesis, a simple pseudo-homogeneous model was developed and confronted with experimental data. No temperature differences between the thermocouples placed in the reactor were observed; correspondingly, an isothermal model seems to be adequate for simulation of the investigated system. The following assumptions were made:

- conditions in the radial direction are uniform;
- liquid hold-up is independent of bed height;
- axial dispersion in the gas- and liquid-phase is negligible;
- gas and liquid flow rates are constant throughout the reactor;

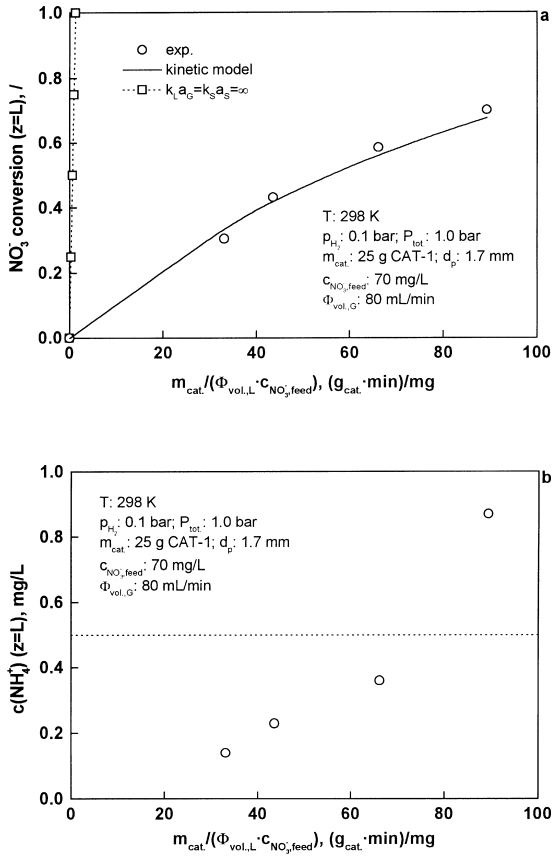

Fig. 5. Measured and calculated nitrate conversion (a) and concentration of ammonium ions (b) as a function of $m_{cat.}/\Phi_{vol.,L} c_{NO_3^-,feed}$ ratio obtained in the bubble-column fixed-bed reactor.

- gas–liquid interfacial area, a_G, is independent of liquid flow rate;
- catalyst particles are completely wet;
- mass-transfer resistance in the gas-phase is negligible, so that equilibrium exists at the gas–liquid interface; and,
- first-order kinetics of catalytic nitrate reduction is proposed.

The model also ignores any variation of hydrogen concentration in the liquid along the reactor; in fact, the hydrogen is continually fed to the liquid from the gas-phase. Considering the above assumptions and appropriate initial and boundary conditions, integration of the respective mass balance equation describing the BCFR reactor results in the following equation:

$$\frac{m_{\text{cat.}}\varepsilon_L k_o}{v\rho_B\varepsilon_B\Phi_{\text{vol.,L}}} = \ln\frac{1}{1 - X_{NO_3^-|z=L}} \quad (1)$$

By using Eq. (1), the predicted nitrate conversion vs. $m_{\text{cat}}/\Phi_{\text{vol.,L}}c_{NO_3^-,\text{feed}}$ is shown in Fig. 5a by a solid curve. It can be seen that good agreement between the measured and calculated values is achieved, which indicates that the assumptions and the reactor model developed are reliable. The average value of the global reaction rate constant, k_0, was found to be equal to $0.01\,s^{-1}$, and independent of the volumetric liquid flow rate for the investigated range. A comparison of the global reaction rate constant with $k_L a_G$ and $k_S a_S$ coefficients was performed in order to elucidate which of the mass-transfer processes governs the catalytic nitrate reduction in the BCFR reactor at the given reaction conditions. In general, the correlations for the prediction of $k_L a_G$ and $k_S a_S$ mass-transfer coefficients in a bubble-column fixed-bed reactor show little agreement with each other, and high percentage differences can be found. Nevertheless, they are adequate to perform an order of magnitude analysis of the global reaction rate constant and the mass-transfer coefficients. Fig. 6a shows the $k_L a_G$ mass-transfer coefficient as a function of superficial liquid velocity. The solid curves were constructed by means of correlations proposed by Reiss [17] and Alexander and Shah [18]. It is evident from Fig. 6a that the calculated values of the reaction rate constant, k_0, are found within a range limited by the curves. Based on this finding, it is concluded that nitrate conversion is retarded only by the hydrogen mass-transfer from the gas- to the bulk liquid-phase,

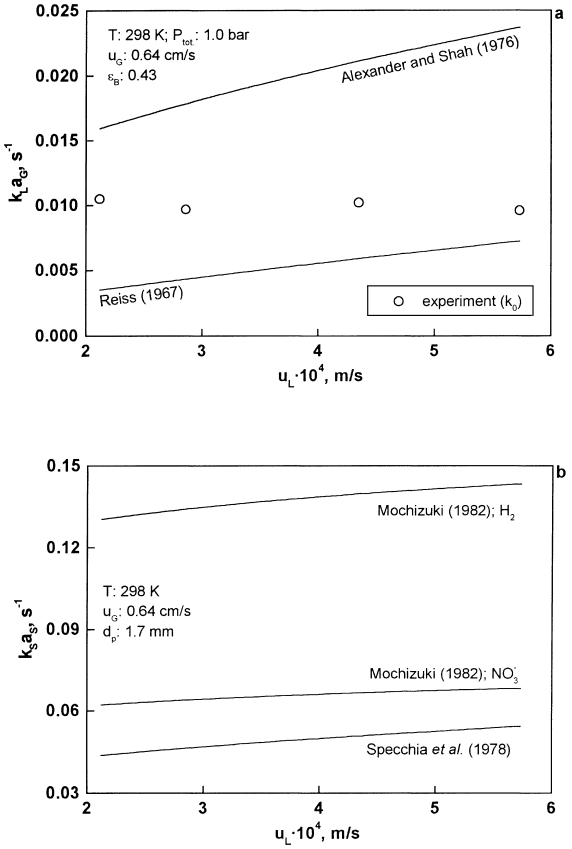

Fig. 6. Influence of superficial liquid velocity on volumetric mass-transfer coefficients: (a) $k_L a_G$; (b) $k_S a_S$.

which could be attributed to the low solubility of hydrogen in water. On the other hand, the values of $k_S a_S$ mass-transfer coefficients proposed by Specchia et al. [19] and Mochizuki [20], are higher than those of $k_L a_G$ coefficients (Fig. 6b). Consequently, the influence of the liquid–solid mass-transfer on catalytic nitrate reduction is negligible at the used operating conditions.

Fig. 5a demonstrates that in the absence of mass-transfer limitations much higher efficiency of the CAT-1 sample could be observed in the process of liquid-phase nitrate hydrogenation. The dashed line in Fig. 5a was constructed on the basis of kinetic data obtained in a gradientless slurry reactor [6]. A comparison of both curves in Fig. 5a reveals that only about 1.5% of the catalyst present in the reactor is efficiently exploited. Based on the above discussion, it is concluded that the catalytic nitrate reduction

carried out in the presence of a highly active Pd–Cu bimetallic catalyst offers an excellent tool for the evaluation of actual $k_L a_G$ coefficients in a bubble-column fixed-bed reactor under reaction conditions.

The influence of hydrogen partial pressure on catalytic nitrate reduction carried out in the BCFR reactor is illustrated in Fig. 7. At the given reaction conditions, complete removal of nitrate ions from the liquid-phase is achieved at $p(H_2) = 0.4$–0.5 bar. It is evident that the production of ammonium ions is particularly enhanced at higher hydrogen partial pressures, which might be attributed to the slow desorption of intermediate products from the catalyst surface. Mass-balance calculations show that at $p(H_2) = 0.05$ bar about 1 mol% of consumed nitrates is converted to ammonium ions; on the other hand, at $p(H_2)$=0.5 bar the amount of nitrogen found in the form of ammonium ions in the reactor effluent increases to 27 mol%. In order to ensure concentrations of ammonium ions in the reactor effluent lower than the prescribed value, the BCFR reactor should operate at $p(H_2) \leq 0.1$ at the employed reaction conditions. Based on Eq. (1), one would expect exponential decay of the outlet nitrate concentration as a function of hydrogen partial pressure. Indeed, it is evident in Fig. 7 that the measured and predicted values of outlet nitrate concentrations are in excellent agreement for hydrogen partial pressures in the range of 0.0–0.3 bar. At higher values of $p(H_2)$, larger deviations between experimental and calculated values are observed. This cannot be attributed to any systematic error in the on-line preparation of the H_2–CO_2 gas-mixture, since it has been verified experimentally and numerically that in the used range of operating conditions the concentrations of both species dissolved in the liquid-phase are linearly proportional to the concentration of H_2 and CO_2 in the gas-phase. Considering the fact that a very simple model was used to simulate the process of catalytic liquid-phase nitrate reduction carried out in the BCFR reactor, it can be concluded that Eq. (1) fits the measured data very well. In these calculations, it was supposed that nitrate disappearance rate is of first order with respect to hydrogen partial pressure. Good agreement between the measured and calculated nitrate outlet concentrations confirms the above derived conclusion that in the BCFR reactor, nitrate reduction is determined by mass-transfer of hydrogen from the gas- to the bulk liquid-phase. For comparison, additional calculations were done in order to check the assumption that the reaction rate might be of one-half order with respect to hydrogen partial pressure. However, the dashed line (obtained by setting the value of global reaction rate constant to $0.01\,s^{-1}$) plotted in Fig. 7 demonstrates that in this case no agreement between the measured and calculated data is achieved. This finding shows again that the BCFR reactor did not operate in the kinetic regime, since hydrogen adsorption, which is typically of one-half order with respect to $p(H_2)$ on noble metal catalysts [21], was masked by gas–liquid mass-transfer resistances.

In this work, the H_2–CO_2 gas-mixture was fed to the BCFR reactor; CO_2 was employed in order to eliminate the influence of stoichiometrically produced hydroxide ions on the reaction course, and to keep the pH value of the aqueous phase constant. Actually, for the operating conditions listed in the caption of Fig. 7, the pH value of the liquid-phase was found to be constant along the catalytic bed as long as nitrate conversion was lower than 0.5; at $X_{NO_3^-} = 1$, the pH value of the liquid-phase at the reactor exit was higher by about one unit when compared to the pH value of the feed solution. The metal loadings in the catalyst employed are relatively low and the metallic clusters are less than 50–70 Å in diameter, because X-ray analysis did not show the metallic phase. Hence, the charging mechanism of the catalytic solid is likely to be controlled by the γ-Al_2O_3 support, and occurs as a result of proton binding/release, which is pH dependent. Since the catalyst surface is in a dynamic equilibrium with the thin liquid film surrounding the catalyst particle, the increase of pH value of the liquid-phase might result in negative charge development, which arises due to the deprotonation of the catalyst surface ($MOH_2^+ \Leftrightarrow MOH + H^+, MOH \Leftrightarrow MO^- + H^+$). Consequently, a build-up of negative charge on the particle surface would result in lower nitrate disappearance rates due to the enhanced coulombic repulsion between unconverted nitrate ions and the catalyst along the reactor tube. Recently, catalyst deprotonation and simultaneous decrease in the activity of alumina supported Pd monometallic and Pd–Cu bimetallic catalysts has been observed in the process of liquid-phase nitrite hydrogenation [22,23]. However, the results presented in Fig. 7 confirm that the increase of pH value of the liquid-phase has no inhibitive effect on the measured

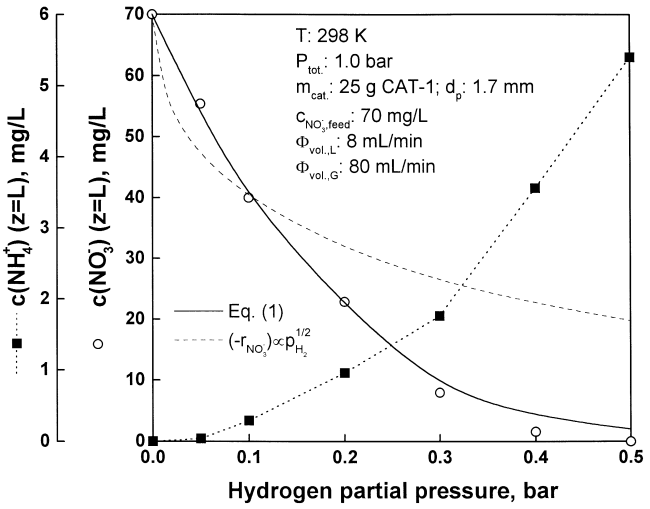

Fig. 7. Nitrate and ammonium ions concentration vs. hydrogen partial pressure dependencies obtained in the BCFR reactor. The dashed line was obtained by assuming nitrate reduction to be of one-half reaction order with respect to hydrogen partial pressure.

nitrate conversions at lower concentrations of CO_2 dissolved in the liquid-phase. This is attributed to the operation of the BCFR reactor in the mass-transfer regime. To conclude, it should be mentioned that the catalyst surface protonation/deprotonation is a reversible process; after increasing the concentration of carbon dioxide in the gas-phase, the catalyst would, if there was any deactivation, recover its activity for nitrate reduction.

Fig. 8a illustrates nitrate conversion as a function of feed nitrate concentration. It can be seen that for $C_{NO_3^-,feed}$ above 70 mg/l, the nitrate conversion increases with the decrease of feed nitrate concentration, as expected from the definition of conversion. For lower values of $C_{NO_3^-,feed}$, the measured nitrate conversions decrease. This might be attributed to liquid–solid mass-transfer resistance, which is due to lower rate of nitrate transport from the bulk liquid-phase to Pd–Cu active sites on the catalyst surface. For the given reaction conditions, it is believed that this resistance increases proportionally with the decrease of feed nitrate concentration. Correspondingly, its effect on the measured nitrate conversions is more pronounced at lower values of $C_{NO_3^-,feed}$, which results in the appearance of maxima observed in Fig. 8a. On the other hand, Fig. 8b indicates that for $C_{NO_3^-,feed}$ above 70 mg/l the concentration of ammonium ions measured in the reactor effluent is almost constant for the given value of hydrogen partial pressure. At lower nitrate feed concentrations, higher contents of ammonium ions were detected. Since less nitrate was reduced at $C_{NO_3^-,feed}$ =60 mg/l, a higher amount of hydrogen adsorbed on the catalyst surface was available for subsequent reaction steps, which resulted in the enhanced formation of ammonium ions. It should be noted that in these runs, the same amount of hydrogen was transferred to the catalyst surface for the given hydrogen partial pressure.

Fig. 9a shows the concentration of unconverted nitrate ions as a function of hydrogen partial pressure obtained in the BCFR reactor in the presence of various Pd–Cu bimetallic catalysts. Although the amounts of metallic phases deposited on γ-Al_2O_3 support were varied in a wide range, no difference in the behavior of employed catalysts was observed, since the reactor was operated in the mass-transfer regime, and the nitrate disappearance rate was determined by mass-transfer of hydrogen from the gas- to the bulk liquid-phase. The activity of CAT 1–3 Pd–Cu bimetallics for nitrate reduction, measured in the BCFR reactor, was equal to 0.55 g/($g_{cat.}$·h), which is in good agreement with the results of Sell et al. [8].

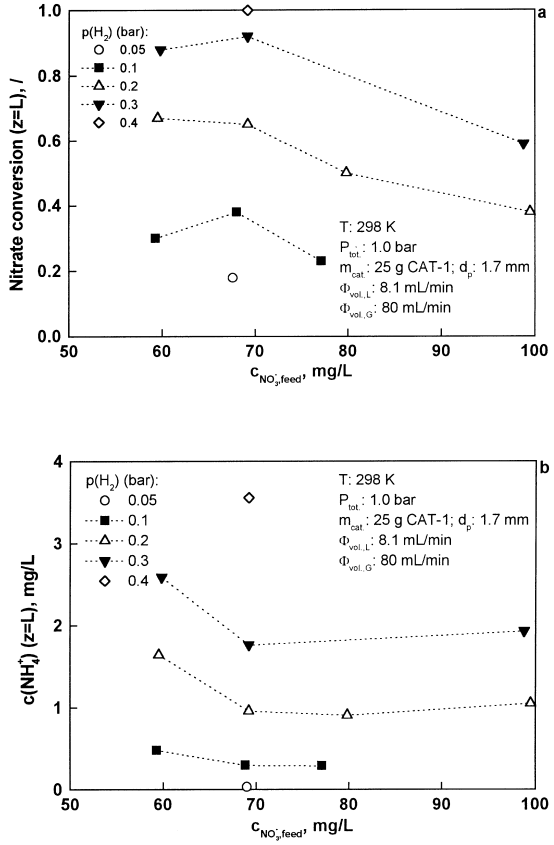

Fig. 8. Nitrate conversion (a) and concentration of ammonium ions (b) as a function of feed nitrate concentration at different hydrogen partial pressures in the BCFR reactor.

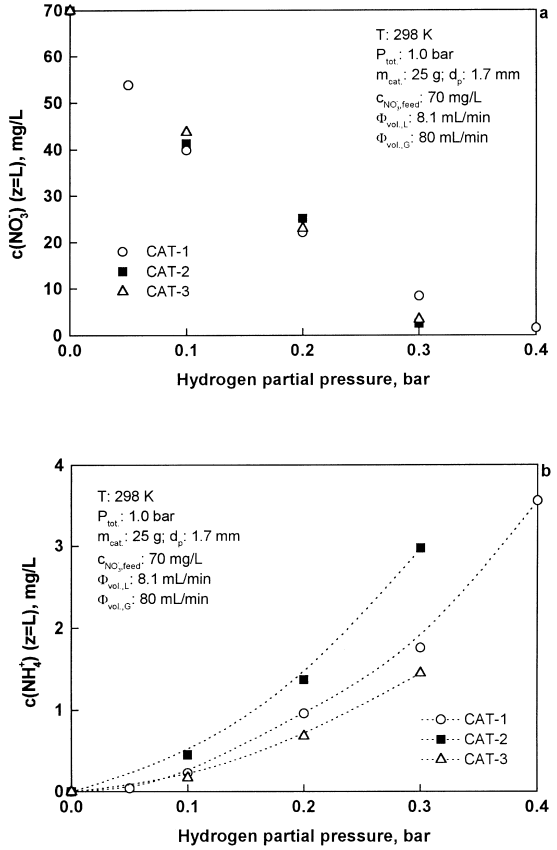

Fig. 9. Outlet nitrate (a) and ammonium (b) ions concentration as a function of hydrogen partial pressure obtained in the BCFR reactor packed with various Pd–Cu bimetallic catalysts.

More interesting results are depicted in Fig. 9b, in which the concentration of ammonium ions formed during the catalytic nitrate reduction is plotted as a function of hydrogen partial pressure. It is evident that the rate of ammonium ions formed decreases in the following order: CAT-2 > CAT-1 > CAT-3. Nitrate reduction carried out over the CAT-3 sample resulted in lower formation of ammonium ions in comparison to CAT-1, since the concentrations of Pd and Cu phases deposited on γ-Al_2O_3 were lower for an order of magnitude. Due to this reason, lower amounts of hydrogen were adsorbed on the catalyst surface. Based on the results illustrated in Fig. 9b and accordingly to our previous results [24], it can be tentatively concluded that in the case of CAT-1 the catalyst surface was enriched with Pd atoms. Batista et al. [24] report that enrichment of the catalyst surface with a noble metal significantly contributes to the selective transformation of intermediate nitrite ions to nitrogen. Based on the observed data, it is believed that in the case of CAT-2 more homogeneous spatial distribution of Pd and Cu metallic phases was obtained, which results in higher production of ammonium ions in comparison to CAT-1.

3.2. Trickle-bed reactor (TBR)

Fig. 10a shows the outlet nitrate concentration *vs.* hydrogen partial pressure dependencies obtained in bubble-column fixed-bed and trickle-bed reactors. The catalyst utilization degree is lower in the trickle-bed reactor, because of the strong hydrodynamic limitations due to the ineffective wetting and mass-transfer effects. For the given reaction conditions, the mean

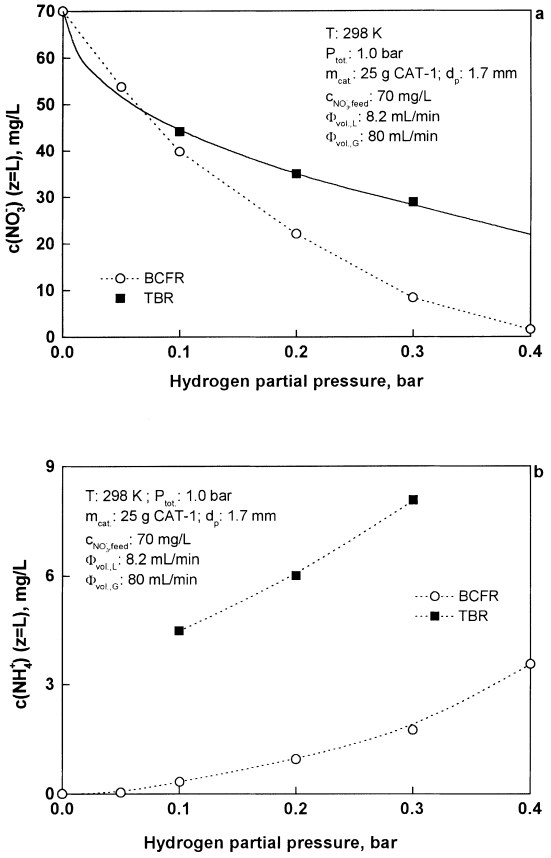

Fig. 10. Nitrate (a) and ammonium (b) ions concentration as a function of hydrogen partial pressure measured in bubble-column fixed-bed and trickle-bed reactors. The solid line was obtained by assuming nitrate reduction in the TBR reactor to be of one-half reaction order with respect to hydrogen partial pressure.

residence time of the liquid-phase in the TBR reactor was estimated to be in the range of 0.5–0.7 min [25]. Furthermore, due to low liquid flow rates, only about 50% of the outer surface of catalyst particles in the TBR reactor, which operated in LIR trickle-flow regime, was partially wet [26]. Catalyst particles were directly exposed to the gas-phase (the amounts of hydrogen adsorbed on the catalyst surface were much higher in comparison to the BCFR reactor), therefore the outlet nitrate concentration is less sensible to the variation of hydrogen partial pressure. For the same reason, one can tentatively conclude that the measured nitrate concentrations in the effluent of the TBR reactor are determined by the mass-transfer of nitrate ions from the bulk liquid-phase to the catalyst surface. It was demonstrated above (Fig. 7) that in the BCFR reactor the nitrate disappearance rate is, due to gas–liquid mass-transfer limitations, of first order with respect to hydrogen partial pressure. Due to the lack of gas-liquid mass-transfer resistance in the case of TBR reactor, which is a consequence of a direct contact of the gas-phase and the catalyst surface, the solid line in Fig. 10a suggests that in this reactor system nitrate reduction is of one-half order with respect to hydrogen partial pressure. In other words, hydrogen adsorbs dissociatively on the surface of CAT-1 Pd–Cu bimetallic catalyst. Based on the results plotted in Fig. 10a, it is believed that for the given range of operating conditions, the performance of the TBR reactor would be advantageous over the BCFR reactor at $p(H_2)$ below 0.07 bar.

It can be seen in Fig. 10b, in which the concentration of ammonium ions is plotted as a function of hydrogen partial pressure, that the production of ammonium ions is drastically enhanced in the TBR reactor. At the given reaction conditions, as much as 65 mol% of consumed nitrates was transformed to ammonium ions. This is again attributed to the partial wetting of catalyst particles in the TBR reactor, which results in comparison to the BCFR reactor in a much higher concentration of adsorbed hydrogen species on the catalyst surface. Correspondingly, subsequent reaction steps leading to the formation of ammonium ions are enhanced.

Additional experiments were carried out in the TBR reactor in which the influence of volumetric liquid flow rate on the reaction course was investigated. The results obtained in the range of employed $\Phi_{vol.,L}$ (Table 2) show that the upflow two-phase reactor gives higher nitrate conversion rates, because of much better effective wetting of the particles. These observations are in agreement with the results of Mazzarino et al. [27], who studied oxidation of ethanol to acetic acid in the liquid-phase on an alumina supported Pd catalyst using the same types of reactors. Furthermore, a comparison of correlations for the prediction of $k_L a_G$ and $k_S a_S$ mass-transfer coefficients in the bubble-column fixed-bed [17,18] and trickle-bed [25,28] reactors demonstrates that even in the case of complete wetting of catalyst particles in the TBR reactor and no flow maldistribution in a catalytic bed, the performance of the BCFR reactor would be better in comparison to the TBR reactor in the given range

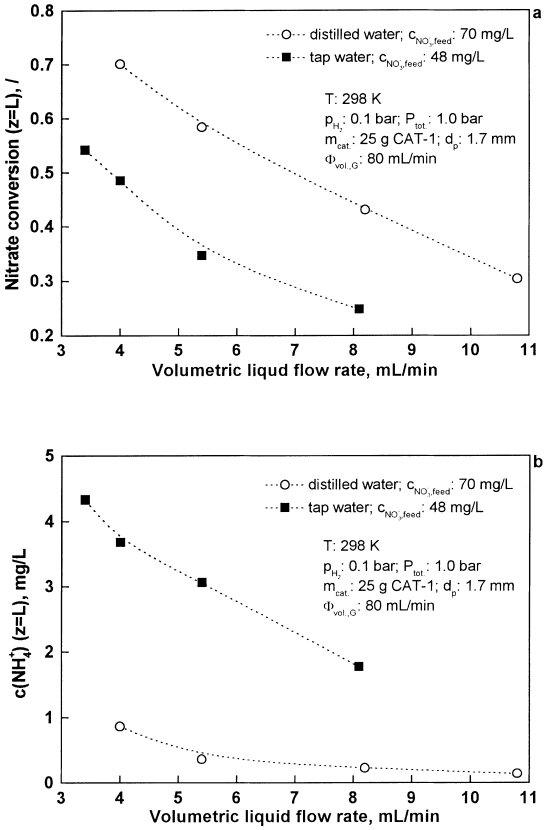

Fig. 11. Nitrate (a) and ammonium (b) ions concentration vs. volumetric liquid flow rate dependencies obtained in the BCFR reactor using different reaction media.

of operating conditions (Table 2). In the latter reactor system, the concentration of ammonium ions decreases with an increase of volumetric liquid flow rate. This is ascribed to higher portion of outer catalyst surface covered with a thin liquid film at increased liquid flow rates.

3.3. Influence of reaction medium on catalytic nitrate reduction

Some experiments of catalytic nitrate reduction were conducted in the BCFR reactor in which drinking water was used as a reaction medium instead of distilled water. Drinking water was used as received, and not spiked with any addition of nitrate salt. The results of this investigation are presented in Fig. 11. It is evident in Fig. 11a that lower nitrate conversions are obtained in the presence of drinking water as a liquid-phase. Since TOC concentration of drinking water is low (Table 3), it is believed that dissolved organic compounds (e.g., humic substances) do not exhibit any appreciable influence on the reaction kinetics. Thus, an inhibitive effect of drinking water on nitrate reduction is therefore due to the presence of various ionic species in the liquid-phase. Furthermore, Fig. 11b demonstrates that the composition of the aqueous phase has a considerable influence on the formation of ammonium ions as a side product; again, the production of ammonium ions is enhanced when using drinking water as a reaction medium. Given these operating conditions, approximately 55 mol% of converted nitrate ions was reduced to ammonia. Accordingly to a previous investigation [7], the decrease of nitrate disappearance rate as well as the increase of ammonium ions formation is attributed to the presence of hydrogencarbonates in water. Pintar et al. [7] report that hydrogencarbonate anions adsorb competitively with nitrates to the Pd–Cu active sites, thus reducing the number of active centers accessible to nitrate ions. Furthermore, the presence of hydrogencarbonates in the Helmholtz layer decreases the desorption rate of intermediates and nitrogen from the catalyst surface, which accelerates the formation of ammonia at levels considerably exceeding the maximum permitted concentration. It is also reported by Pintar et al. [7] that permanent hardness of drinking water exhibits no inhibitive impact either on the extent of nitrate removal or on reaction selectivity. Besides excessive amounts of ammonium ions found in the reactor effluent, intermediate nitrite ions were also detected in treated drinking water in quantities higher than the maximum contaminant concentration (i.e., 0.02 mg/l). Furthermore, it should be mentioned that the formation of hydroxylamine was not observed in any of the runs performed in this work, in spite of the reaction medium used (the detection limit of the applied spectrophotometric determination with *p*-nitrobenzaldehyde was equal to 0.01 mg/l NH_2OH).

Since the production of ammonium ions is favored even at low hydrogen partial pressure (0.1 bar), it can be concluded that by using up-to-date Pd–Cu bimetallic catalysts, direct treatment of contaminated drinking water containing higher concentrations of hydrogencarbonate ions seems to be unfeasible. To overcome the drawbacks associated with direct removal of

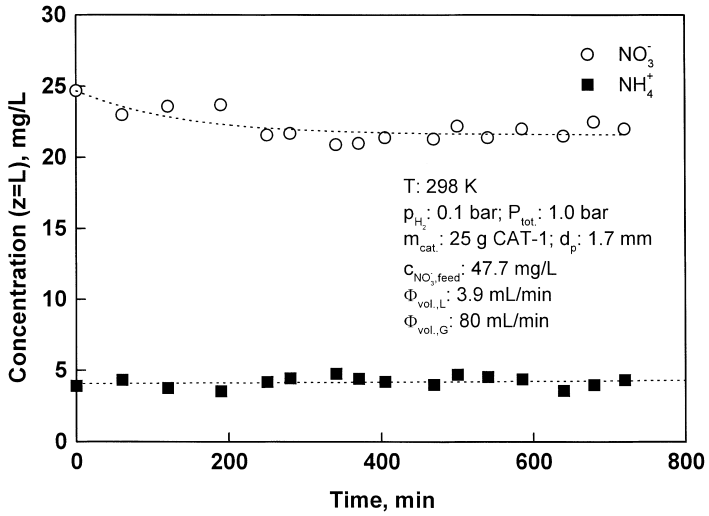

Fig. 12. Nitrate and ammonium ions concentration vs. time-on-stream curves obtained in the BCFR reactor in the course of liquid-phase nitrate reduction using drinking water as a reaction medium.

nitrate ions by means of catalytic hydrogenation, an integrated process has been invented, which efficiently combines the conventional single-bed ion-exchange unit with a catalytic denitrification reactor [29].

3.4. Catalyst stability

Finally, the chemical stability of the Pd–Cu bimetallic catalysts used in this work was tested. For that purpose, the amounts of leached palladium and copper ions in aqueous-phase samples were determined by means of an ICP-AES method. In all samples, the concentrations of metal ions were found to be below the detection limits of both elements. Furthermore, the bulk chemical analysis of fresh and used CAT 1–3 samples confirmed that no dissolution of active components took place during the above described experiments. To demonstrate the chemical resistance of Pd–Cu/γ-Al_2O_3 bimetallic catalyst, a long-term reduction run carried out in the presence of CAT-1 sample is illustrated in Fig. 12. It is evident that after achieving steady-state operation, the concentrations of nitrate and ammonium ions measured in the effluent of the BCFR reactor were independent of time-on-stream. One should note that about 3–7 h were required to obtain a steady-state operation of the BCFR reactor after a step change of reaction conditions; longer time periods were needed particularly when appreciable variations of hydrogen partial pressure were applied. This is attributed to low molar fluxes of nitrate ions to the reactor inlet as well as the observed ability of the employed Pd–Cu bimetallic catalysts for the exchange of nitrate ions with surface functionalities of the alumina support. In this regard, the small drop in outlet nitrate concentration noticed in the first part of $C_{NO_3^-}$ versus time-on-stream dependence shown in Fig. 12, and the time lag of about 200 min needed in order to obtain constant nitrate concentration in the reactor effluent are not surprising.

4. Conclusions

The nitrate disappearance rate in a bubble-column fixed-bed reactor is mainly determined by the mass transfer of hydrogen from the gas- into the bulk liquid-phase. At the given reaction conditions, only about 1–10% of the Pd–Cu/γ-Al_2O_3 bimetallic catalysts present in the reactor is efficiently exploited. Experiments in which the effect of volumetric liquid flow rate on nitrate conversion was investigated, show that the apparent reaction rate is of first order with respect to both nitrate and hydrogen.

In a trickle-bed reactor, lower nitrate conversions were obtained due to the maldistribution of the

liquid-phase. Since the outer surface of catalyst particles was partially wet at the used operating conditions, nitrate was preferentially transformed to ammonium ions.

When drinking water was used as a reaction medium instead of distilled water, the nitrate disappearance rate and reaction selectivity decreased appreciably, which might be ascribed to the presence of hydrogencarbonates in the feed solution. In these runs, nitrite was detected in the reactor effluent at levels higher than the maximum admissible concentration.

The results of this study indicate that the use of up-to-date alumina supported Pd–Cu bimetallics for direct purification of contaminated drinking water with a high level of temporary hardness does not allow selective nitrate removal. In this respect, the composition as well as synthesis of bimetallic solids should be further optimized in order to decrease or avoid the formation of ammonium ions. Development of integrated processes, which combine physico-chemical and catalytic methods, also seems to be promising in order to overcome drawbacks associated with direct denitrification by means of catalytic hydrogenation. In addition, catalytic nitrate reduction should be carried out in such reactors, which enable more efficient contact between reactants and the catalyst surface than conventional fixed-bed reactors.

5. Nomenclature

a_G	gas–liquid interfacial area, m^2/m^3
a_S	total external surface area of particles, m^2 (particles)/m^3 (bed volume)
c	concentration of liquid reactant in liquid, mg/l
d_p	average catalyst particle diameter, mm
$k_L a_G$	volumetric mass-transfer coefficient from gas to liquid, s^{-1}
k_0	global reaction rate constant, s^{-1}
$k_S a_S$	volumetric mass-transfer coefficient from liquid to particle, s^{-1}
L	total length of packed bed, cm
$m_{cat.}$	mass of catalyst in bed, g
p_{H_2}	hydrogen partial pressure, bar
$P_{tot.}$	total operating pressure, bar
$-r_{NO_3^-}$	nitrate disappearance rate, mg/($g_{cat.}$ min)
T	reaction temperature, K
u	superficial velocity, m/s
$X_{NO_3^-}\|_{z=L}$	nitrate conversion in reactor effluent, dimensionless
z	axial coordinate in reactor tube, cm

5.1. Greek

ε_B	void fraction in the bed, dimensionless
ε_L	liquid hold-up, dimensionless
$\Phi_{vol.}$	volumetric flow rate, ml/min
ν	hydrogen-to-nitrate stoichiometric ratio (=2.5), dimensionless
ρ_B	bulk density of particles in bed, g/cm^3

5.2. Subscripts

feed	feed solution
G	gas-phase
L	liquid-phase

5.3. Acronyms

BCFR	bubble-column fixed-bed reactor
LIR	low interaction regime
TBR	trickle-bed reactor

Acknowledgements

Financial support from the Slovenian Ministry of Science and Technology under Grant No. J2-0686 is gratefully acknowledged. The authors also thank the Nikki-Universal Co., Ltd. (Tokyo, Japan), for providing the alumina support used in the present study.

References

[1] A. Kapoor, T. Viraraghavan, J. Environ. Eng. 123 (1997) 371.
[2] K.D. Vorlop, T. Tacke, M. Sell, G. Strauss, DE 3830850 A1, European Patent Office, 10 September, 1988.
[3] K.D. Vorlop, T. Tacke, Chem. Ing. Tech. 61 (1989) 836.
[4] S. Hörold, K.D. Vorlop, T. Tacke, M. Sell, Catal. Today 17 (1993) 21.

[5] U. Prüsse, S. Hörold, K.D. Vorlop, Chem. Ing. Tech. 69 (1997) 93.
[6] A. Pintar, J. Batista, J. Levec, T. Kajiuchi, Appl. Catal. B: Environ. 11 (1996) 81.
[7] A. Pintar, M. Šetinc, J. Levec, J. Catal. 174 (1998) 72.
[8] M. Sell, M. Bischoff, D. Bonse, Vom Wasser 79 (1992) 129.
[9] P.A. Cawse, Analyst 92 (1967) 311.
[10] H. Müller, B. Frey, B. Schweizer, Techniques for Flow Injection Analysis in UV/Vis Spectroscopy, Perkin-Elmer, Überlingen, 1992.
[11] D.P. Johnson, Anal. Chem. 40 (1968) 647.
[12] A. Pintar, T. Kajiuchi, Acta Chim. Slovenica 42 (1995) 431.
[13] A.L. Marquez, F. Larachi, G. Wild, A. Laurent, Chem. Eng. Sci. 47 (1992) 3485.
[14] F. Larachi, A. Laurent, N. Midoux, G. Wild, Chem. Eng. Sci. 46 (1991) 1233.
[15] E.J. Molga, K.R. Westerterp, Ind. Eng. Chem. Res. 36 (1997) 622.
[16] E.J. Molga, K.R. Westerterp, Chem. Eng. Process. 36 (1997) 489.
[17] L.P. Reiss, Ind. Eng. Chem. Proc. Des. Dev. 6 (1967) 486.
[18] B.F. Alexander, Y.T. Shah, Can. J. Chem. Eng. 54 (1976) 556.
[19] V. Specchia, G. Baldi, A. Gianetto, Ind. Eng. Chem. Proc. Des. Dev. 17 (1978) 362.
[20] S. Mochizuki, Chem. Eng. Sci. 37 (1982) 1422.
[21] Z. Knor, Chemisorption of Dihydrogen, in: J.R. Anderson, M. Boudart (Eds.), Catalysis-Science and Technology, Vol. 3, Akademie-Verlag, Berlin, 1983, p. 231.
[22] A. Pintar, J. Batista, J. Levec, Wat. Sci. Tech. 37 (1998) 177.
[23] A. Pintar, G. Berčič, J. Levec, AIChE J. 44 (1998) 2280.
[24] J. Batista, A. Pintar, M. Čeh, Catal. Lett. 43 (1997) 79.
[25] S. Goto, J.M. Smith, AIChE J. 21 (1975) 706.
[26] C.N. Satterfield, AIChE J. 21 (1975) 209.
[27] I. Mazzarino, M. Occhetti, G. Baldi, S. Sicardi, Chem. Eng. Comm. 75 (1989) 225.
[28] A. Dharwadkar, N.D. Sylvester, AIChE J. 23 (1977) 376.
[29] A. Pintar, J. Batista, G. Berčič, J. Levec, P-9800182, SI Patent Application, June 26 (1998).